Eurasian Journal of Physics and Functional Materials

2026, 10(4), 425-444

Computer modeling of the electronic properties of reduced-dimensionality structures based on NaCl nanocrystals

A.S. Istlyaup[1,*], L.N. Myasnikova[1], A. Lushchik[2]

[1]Faculty of Physics and Matematics, K. Zhubanov Aktobe Regional University, Aktobe, Kazakhstan

[2]Institute of Physics, University of Tartu, Tartu, Estonia

E-mail: aistlyaup@zhubanov.edu.kz

DOI: **10.32523/ejpfm.2026100406**
Received: 4 June 2026
Revised: 13 October 2026
Accepted: 10 November 2026

This study presents a computational investigation of the electronic characteristics of reduced-dimensional NaCl structures with different atomic geometries, including linear, planar, three-dimensional, structurally modified, and nanotube configurations. The calculations were performed using the Atomistix ToolKit/Virtual NanoLab environment within a periodic supercell representation. The calculated k-dependent electronic spectra, density of states (DOS), and Kohn–Sham electronic gaps were analyzed with respect to atomic geometry, dimensionality, and structural modification. For the investigated linear, planar, and three-dimensional NaCl configurations, the calculated electronic gaps range from approximately 8.45 to 12.09 eV and exhibit no simple monotonic dependence on the number of ions, indicating that the electronic spectrum is strongly influenced by the particular atomic arrangement and simulation-cell geometry. Removal of one Na-Cl pair from the parent $Na_{14}Cl_{13}$ configuration, resulting in the $Na_{13}Cl_{12}$ model, is accompanied by a redistribution of electronic states and yields a calculated electronic gap of approximately 9.01 eV. For the periodic NaCl nanotube models (4,1), (5,1), and (6,1), the calculated electronic gaps are approximately 6.40, 5.32, and 5.00 eV, respectively. A systematic decrease in the electronic gap is therefore observed across the investigated nanotube series; however, this trend is not attributed to a single structural parameter because the models also differ in atom number and simulation-cell dimensions. Overall, the results demonstrate that the calculated electronic characteristics of the investigated NaCl models are sensitive to atomic geometry, dimensionality, and structural configuration.

Keywords: NaCl nanostructures; reduced-dimensional structures; electronic structure; density of states; Kohn–Sham electronic spectrum; periodic supercell; NaCl nanotubes.

1. Introduction

Alkali halides constitute an important class of ionic solids formed by alkali-metal cations and halide anions. Their relatively simple crystal structures and predominantly ionic bonding make them useful model systems for investigating fundamental relationships between atomic structure and electronic properties [1, 2]. Bulk alkali halides are generally wide-gap insulating materials, and their electronic structure, optical response, and excitation processes have been extensively investigated experimentally and theoretically [3–8]. Among them, NaCl represents one of the simplest and most extensively studied ionic crystals and therefore provides a convenient reference system for examining how changes in atomic arrangement and dimensionality affect electronic characteristics [2, 9].

The electronic characteristics of ionic materials can be modified by changes in atomic coordination, structural geometry, composition, and dimensionality. Such modifications alter the local environment of the constituent ions and may consequently change the distribution of occupied and unoccupied electronic states and the corresponding electronic energy gaps [10–12]. These effects become particularly relevant in reduced-dimensional systems, where atomic arrangements and boundary conditions can differ substantially from those of the corresponding bulk crystal [10, 13]. Computational electronic-structure methods therefore provide an important means of examining structure–property relationships in alkali halide systems with different geometrical organizations [11, 12].

Particular interest has been directed toward reduced-dimensional alkali halide structures, in which changes in atomic coordination and structural geometry can produce electronic characteristics that differ from those of the corresponding bulk crystals [11–13]. Depending on their atomic organization, nanoscale systems may exhibit zero-, one-, or two-dimensional structural motifs, including compact clusters, chains, sheets, and tubular configurations. Previous theoretical studies have shown that the structural and electronic properties of alkali halide nanosystems can vary with composition, size, and geometry [11–15]. These observations provide motivation for systematic computational studies of how different atomic arrangements affect the electronic characteristics of reduced-dimensional NaCl structures.

NaCl has been investigated in a variety of reduced-dimensional structural forms, including finite clusters, chain-like and planar configurations, and tubular structures [11, 12]. Previous theoretical studies have demonstrated that the calculated electronic characteristics of such NaCl-based systems can differ from those of bulk crystalline NaCl and can vary with atomic arrangement, system size, local coordination, and the adopted computational representation [16, 17]. These structural forms should be distinguished from one another because they correspond to different atomic geometries and boundary conditions. In particular, finite clusters, periodic low-dimensional configurations, and nanotubes should not be treated as physically equivalent models. Consequently, comparison of their calculated electronic structures provides a means of examining relationships between atomic organization and electronic characteristics in reduced-dimensional ionic systems.

Tubular alkali halide structures have received considerable theoretical attention as a distinct class of reduced-dimensional ionic systems [16–18]. Previous computational studies have investigated tubular configurations based on LiF, NaF, NaCl, KBr, and related alkali halides and have demonstrated that their structural and electronic characteristics depend on chemical composition, size, and geometrical organization [16, 17]. Calculations performed for tubular LiF, NaCl, and KBr structures have shown that different tubular geometries can be realized within the investigated model systems and that their relative properties vary with structural configuration [16]. More recently, the density of states and band structure of NaF nanotubes have been investigated computationally, revealing systematic differences in the calculated electronic characteristics among different tubular configurations [17]. Computational studies of low-dimensional alkali-halide-containing systems, including alkali metal iodide structures encapsulated within carbon nanotubes, have further demonstrated the sensitivity of their electronic characteristics to structural organization and composition [18]. Together, these studies establish a basis for extending comparative electronic-structure analysis to different geometrical configurations of NaCl.

Despite previous theoretical studies of individual alkali halide nanostructures and tubular configurations [18–21], a comparative analysis of the calculated electronic characteristics of NaCl models with substantially different atomic geometries within a common computational framework remains relevant. In the present work, linear, planar, three-dimensional, structurally modified, and nanotube NaCl configurations represented within periodic computational cells are investigated. The analysis focuses on their k-dependent Kohn–Sham electronic spectra, total density of states, and calculated electronic gaps, with particular attention to variations associated with atomic arrangement, dimensionality, and structural modification. For the nanotube models, the (4,1), (5,1), and (6,1) configurations are considered. The aim of the present work is to determine how differences in structural organization are reflected in the calculated electronic characteristics of reduced-dimensional NaCl models and to identify systematic trends that can be established within the limitations of the employed computational representation.

2. Material and methods

The computational description of nanoscale systems depends on the boundary conditions and periodicity adopted in the model. In the present work, the investigated linear, planar, three-dimensional, and nanotube NaCl configurations were represented within periodic simulation cells in Atomistix ToolKit (ATK). The lattice vectors, cell dimensions, and internal atomic arrangements were defined separately for each investigated configuration according to its particular geometry. Consequently, the calculated electronic states and the corresponding reciprocal-space characteristics are interpreted within the periodic computational representation defined for each model [22, 23].

The investigated NaCl models were classified according to the spatial organi-

zation of Na and Cl atoms within the corresponding simulation cells. The terms linear, planar, and three-dimensional therefore describe the atomic geometry of the model rather than its boundary conditions. Periodic tubular NaCl configurations were considered as a separate structural class and are referred to as nanotube models throughout the work. Thus, the geometrical classification used here should not be interpreted as implying that the linear or planar configurations are isolated finite clusters or non-periodic systems. All investigated structures are treated according to their actual periodic computational representation, while the terms linear, planar, three-dimensional, and nanotube are used exclusively to distinguish their atomic arrangements.

The linear NaCl configurations contained 2, 4, 6, or 12 ions, corresponding to NaCl, Na_2Cl_2, Na_3Cl_3, and Na_6Cl_6 compositions, respectively. The planar configurations contained 4, 6, 8, or 12 ions, while the three-dimensional configurations contained 8 or 12 ions. Each configuration was placed in an explicitly defined periodic simulation cell, with the lattice dimensions selected according to the geometry and composition of the particular model. The simulation-cell dimensions therefore differed among the investigated configurations. Since a systematic convergence study with respect to the dimensions of the simulation cell and the separation between neighboring periodic replicas was not performed, these dimensions are regarded as parameters of the adopted computational representation and are not interpreted as demonstrating complete isolation between periodic images.

For a periodic system, translational symmetry allows the electronic states to be characterized by a wave vector k, resulting in a k-dependent electronic spectrum within the corresponding Brillouin zone [22]. Since all NaCl configurations investigated in the present work were represented by periodic simulation cells, their calculated electronic spectra were analyzed within this reciprocal-space framework. The Brillouin zone and the relevant reciprocal-space directions are determined by the lattice vectors of each particular simulation cell. Consequently, the k-space paths used for the investigated linear, planar, and three-dimensional configurations are associated with their individual periodic cells and should not be interpreted as the conventional high-symmetry paths of bulk rock-salt NaCl. The specific reciprocal-space paths employed in the electronic-spectrum calculations are given below.

Changes in atomic coordination and geometrical arrangement can modify the local electronic environment of reduced-dimensional ionic structures [11, 12, 16]. In the present work, the resulting differences among the investigated NaCl configurations were characterized using the calculated k-dependent electronic spectra and total density of states. The total DOS was analyzed as the energetic distribution of the calculated electronic states and was used to compare the overall spectral characteristics of different configurations. However, total DOS alone does not provide spatial or atom-specific information. It was therefore not used to assign atomic charges, determine orbital or real-space localization of particular states, identify specific defect-localized states, or quantify the degree of ionicity. Such interpretations would require additional analyses, such as atom- or orbital-resolved DOS, charge-density distributions, or an appropriate charge-partitioning

procedure, which were not performed in the present work.

The electronic-structure calculations were performed using the Quantum Wise Atomistix ToolKit within the Virtual NanoLab (VNL) environment, version 2015.1 [23]. The linear, planar, and three-dimensional NaCl configurations were implemented using the ATK Bulk Configuration representation and treated with an LCAO calculator. According to the preserved input files, the electronic temperature for these calculations was explicitly set to 1 K. The preserved scripts do not explicitly define the exchange–correlation functional, basis set, pseudopotential set, mesh cutoff, spin-polarization settings, or a user-defined SCF convergence tolerance for these configurations. Since these parameters cannot be unambiguously reconstructed from the available calculation files, no specific values are retrospectively assigned to them in the present description. Parameters that are explicitly available for the nanotube calculations are reported separately below.

The density of states and the k-dependent electronic spectra were evaluated as separate electronic-structure analyses. In the preserved ATK analysis scripts, the DOS calculations for the linear, planar, and three-dimensional configurations were performed using a $1 \times 1 \times 1$ Monkhorst–Pack grid [24]. The k-dependent electronic spectra were calculated independently using the ATK Bandstructure analysis object along predefined paths in reciprocal space, with 20 points specified for each path segment. The selected reciprocal-space paths depended on the lattice vectors and geometry of the particular periodic simulation cell and therefore were not identical for all investigated configurations. Accordingly, the $1 \times 1 \times 1$ grid specified for the DOS analysis should not be interpreted as the reciprocal-space sampling used to generate the k-dependent electronic spectra. The specific paths used for the individual configurations are reported below where they can be reconstructed from the preserved analysis scripts.

For the investigated linear, planar, and three-dimensional configurations, the reciprocal-space paths used for the k-dependent electronic-spectrum calculations were defined individually according to the lattice vectors of the corresponding periodic simulation cells. Depending on the particular model, the preserved analysis scripts specify the paths Z – Γ – Z, A – Γ – X, A – Γ – X – Z – L – B, and Γ – L – Z, with 20 points specified for each path segment. Since the investigated configurations were represented by different simulation cells, the reciprocal-space labels and paths are specific to the lattice of each computational model. They should therefore not be interpreted as the conventional high-symmetry path of bulk rock-salt NaCl.

In addition to the linear, planar, and three-dimensional NaCl configurations, periodic tubular NaCl structures were investigated as a separate structural class. The nanotube series considered in the present work consists of the (4,1), (5,1), and (6,1) configurations. In this notation, the second index n remains fixed at 1, whereas the first index m increases from 4 to 6 across the investigated series. The nanotube models were represented within periodic simulation cells and were analyzed in terms of their k-dependent electronic spectra and total density of states. Because the three nanotube configurations also differ in the number of atoms and simulation-cell dimensions, they are treated as a series of distinct computational models rather than as systems differing in a single independently

varied geometrical parameter.

Prior to the electronic-structure calculations, the NaCl nanotube configurations were structurally relaxed in ATK using the classical interatomic potential Lusvardi_SiP_NaCaOF_2008 [23]. A force criterion of 0.05 $\mathrm{eV} \cdot \mathrm{Å}^{-1}$ was specified for the geometry optimization. For the configurations subsequently used in the electronic-structure calculations, the maximum residual force was approximately 0.038 $\mathrm{eV} \cdot \mathrm{Å}^{-1}$. The resulting structures are therefore referred to throughout this work as optimized nanotube configurations. Importantly, this structural relaxation was performed using the specified classical interatomic potential and should not be interpreted as a DFT geometry optimization.

No phonon or vibrational-frequency calculations, finite-temperature molecular-dynamics simulations, or formation- or cohesive-energy analyses were performed for the investigated nanotube models. Consequently, the geometry-optimization results are not interpreted as evidence of their dynamical or thermodynamic stability. The term "optimized nanotube configuration" used in the present work refers only to the structures obtained after the geometry-relaxation procedure described above. Establishing dynamical or thermodynamic stability would require additional calculations beyond the scope of the present study.

The total density of states was used to compare the energetic distribution of calculated electronic states among the investigated configurations. Particular attention was paid to changes in the distribution of occupied and unoccupied states associated with differences in atomic geometry and structural configuration. Comparisons were based on the spectral distribution of the total DOS rather than on its absolute magnitude, since the investigated models contain different numbers of atoms and, consequently, different total numbers of electronic states. As noted above, the total DOS was not used to assign atomic-orbital character, spatial localization, charge redistribution, or the degree of ionicity.

Following geometry optimization, the electronic-structure calculations for the nanotube models were performed within the DFT-LCAO framework [24–26]. The preserved nanotube input files explicitly specify the generalized-gradient approximation using the Perdew–Burke–Ernzerhof (GGA-PBE) exchange–correlation functional and Double-Zeta Polarizedbasis sets for both Na and Cl [23, 28]. The electronic temperature was set to 1 K. The simulation-cell dimensions were defined separately for the (4,1), (5,1), and (6,1) nanotube configurations, as specified below. Computational parameters that are not explicitly defined in the preserved nanotube input files are not assigned retrospectively.

The three nanotube configurations differed in both the number of atoms and the dimensions of the periodic simulation cell. The (4,1) nanotube model contained 28 atoms, corresponding to $Na_{14}Cl_{14}$, and was represented by a simulation cell with $a = b = 13.5898$ Å and $c = 6.5112$ Å. The (5,1) configuration contained 124 atoms ($Na_{62}Cl_{62}$), with $a = b = 14.3616$ Å and $c = 23.7330$ Å, whereas the (6,1) configuration contained 172 atoms ($Na_{86}Cl_{86}$), with $a = b = 15.1368$ Å and $c = 27.9516$ Å. Thus, the investigated nanotube series involves simultaneous changes in geometrical index, system size, and simulation-cell dimensions. These differences are taken into account when interpreting variations in the calculated electronic characteristics of the three nanotube models.

The optimized (4,1), (5,1), and (6,1) nanotube models contained 28, 124, and 172 atoms, corresponding to $Na_{14}Cl_{14}$, $Na_{62}Cl_{62}$, and $Na_{86}Cl_{86}$, respectively. The simulation-cell dimensions were $a = b = 13.5898$ Å and $c = 6.5112$ Å for (4,1), $a = b = 14.3616$ Å and $c = 23.7330$ Å for (5,1), and $a = b = 15.1368$ Å and $c = 27.9516$ Å for (6,1). Because these models differ simultaneously in geometrical index, number of atoms, and simulation-cell dimensions, changes in their calculated electronic properties are interpreted as trends within the investigated model series rather than as effects of a single independently varied structural parameter.

For the periodic NaCl nanotubes, the k-dependent electronic spectra were analyzed in terms of the Kohn–Sham eigenvalues $E_n(k)$ along predefined reciprocal-space paths [26]. For all three nanotube models, the preserved ATK Bandstructure analysis specifies the path A – C – B – Γ – Y – X – Z – L, with 20 points specified for each path segment. The calculated spectra were used to characterize the distribution of occupied and unoccupied Kohn–Sham states and to determine the corresponding calculated electronic gaps. As for the linear, planar, and three-dimensional NaCl configurations, the band-structure analysis was performed separately from the total DOS calculation.

For the nanotube models, the total DOS was evaluated separately using a $1 \times 1 \times 1$ Monkhorst–Pack grid [24], as specified in the preserved analysis scripts. Accordingly, this grid refers specifically to the DOS analysis and not to the reciprocal-space path used for calculation of the k-dependent electronic spectra. The DOS and k-dependent spectra were therefore considered complementary descriptors of the calculated electronic structure.

The calculated k-dependent Kohn–Sham electronic spectra, total density of states, and electronic gaps were compared among the investigated linear, planar, three-dimensional, structurally modified, and nanotube NaCl configurations in order to identify systematic variations associated with differences in atomic organization and structural configuration. Since the investigated models differ simultaneously in several structural and computational parameters, including atomic arrangement, number of atoms, and simulation-cell dimensions, the observed variations are interpreted as comparative trends within the considered model set rather than as dependencies on a single independently varied geometrical parameter. The analysis is restricted to the electronic-structure descriptors directly obtained from the calculations. In particular, the total DOS is not used by itself to infer atomic charge, spatial localization, orbital character, or degree of ionicity, while the geometry-optimization results are not interpreted as evidence of dynamical or thermodynamic stability.

A structurally and compositionally modified NaCl configuration was also considered separately. The $Na_{13}Cl_{12}$ model was obtained from the parent $Na_{14}Cl_{13}$ configuration by removal of one Na-Cl pair while retaining the periodic computational representation. The resulting model was analyzed using the same types of electronic-structure descriptors as the other NaCl configurations, namely the k-dependent electronic spectrum and total DOS. The modification is treated here as a change in atomic composition and structural configuration; no specific defect charge state or localized defect-center assignment is assumed.

3. Results and discussion

Bulk NaCl crystallizes in the rock-salt structure and is conventionally described within the band-theory framework associated with its face-centered-cubic lattice. The upper valence states are predominantly associated with Cl $3p$ states, whereas the lowest conduction states have mainly Na $3s$ character [2–6]. In the present calculations, however, the investigated reduced-dimensional NaCl configurations are represented by periodic simulation cells whose lattice vectors and reciprocal-space descriptions are determined by the geometry of each particular model. Consequently, the conventional high-symmetry-point description of bulk rock-salt NaCl is not directly transferable to the calculated electronic spectra of these configurations.

Figure 1 presents the calculated k-dependent Kohn–Sham electronic spectra of the investigated linear NaCl configurations represented within periodic simulation cells. The models differ in composition, number of ions, internal atomic arrangement, and simulation-cell dimensions. The corresponding calculated electronic gaps are summarized in Table 1. Throughout the following discussion, these quantities are referred to as Kohn–Sham electronic gaps in order to distinguish them from the experimental fundamental band gap of bulk crystalline NaCl.

For the converged linear configurations, the calculated electronic spectra show no monotonic variation of the electronic gap with the number of ions in the simulation cell. Instead, differences in the calculated gaps occur simultaneously with changes in composition, atomic arrangement, and simulation-cell geometry. The present dataset therefore does not support interpretation of the electronic gap as a function of ion number alone. The preserved calculation for the two-ion NaCl configuration did not reach self-consistent-field convergence within the specified maximum number of iterations. Consequently, the previously reported gap value for this configuration was excluded from the quantitative comparison and is not used in the discussion of structural trends.

For the planar NaCl configurations, the calculated Kohn–Sham electronic gaps are 11.83 eV for Na_2Cl_2, 11.46 eV for Na_3Cl_3, 11.55 eV for Na_4Cl_4, and 12.09 eV for Na_6Cl_6. For the three-dimensional configurations, the corresponding values are 11.92 eV for Na_4Cl_4 and 11.12 eV for Na_6Cl_6 (Figure 2 and Table 1). These values do not exhibit a monotonic dependence on the number of ions. Instead, differences in the calculated electronic gaps occur together with differences in atomic arrangement and simulation-cell geometry. The present results therefore show that the number of ions alone is insufficient to account for the observed variations in the calculated electronic spectra.

Experimental investigations of crystalline NaCl have established its wide-gap insulating character and revealed distinct features associated with interband optical transitions and electronic excitations [5–9]. A commonly quoted experimental bulk-gap scale is approximately 8.6 eV, although the precise quantity must be distinguished from excitonic optical features and defined according to the measurement employed. The calculated Kohn–Sham gaps obtained for the present periodic simulation-cell models should not be regarded as direct theoretical

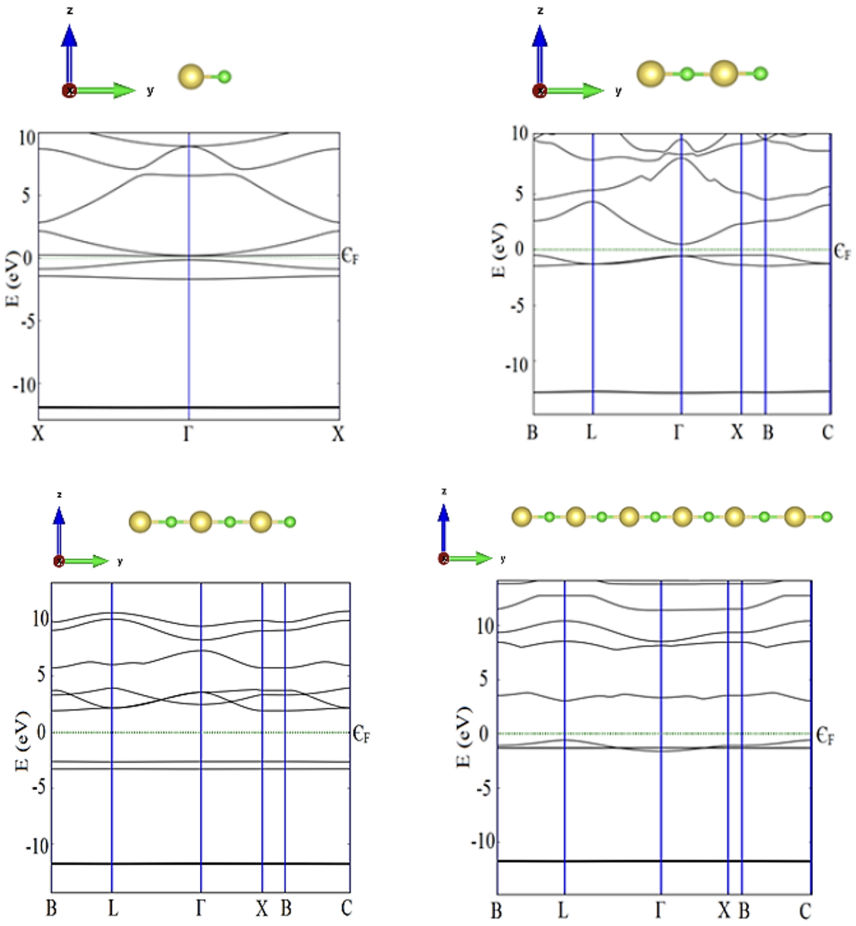

Figure 1. Calculated k -dependent Kohn–Sham electronic spectra of linear NaCl configurations represented within periodic simulation cells. The spectrum of the two-ion NaCl configuration is shown for completeness; the corresponding SCF calculation did not reach convergence within the specified maximum number of iterations and was therefore excluded from the quantitative comparison of electronic gaps.

estimates of an experimental bulk fundamental gap. The investigated configurations differ from bulk rock-salt NaCl in their atomic geometry, simulation-cell symmetry, and periodic representation, and the calculated Kohn–Sham gap is itself dependent on the computational description. Therefore, numerical differences between the present calculated gaps and experimental bulk values are not interpreted as a direct measure of the accuracy of the individual models. The calculated gaps are used primarily for comparative analysis among the investigated NaCl configurations.

A more direct indication of the relationship between atomic arrangement and the calculated electronic spectrum is obtained by comparing configurations with identical composition but different spatial geometries. For Na_4Cl_4, the calculated Kohn–Sham electronic gap changes from 11.55 eV for the planar configuration to 11.92 eV for the three-dimensional configuration. For Na_6Cl_6, the corresponding values are 12.09 and 11.12 eV, respectively. Thus, configurations containing the same numbers of Na and Cl ions can exhibit different calculated electronic gaps when their atomic arrangements and periodic simulation cells differ. Previous investigations of alkali halide clusters likewise establish that structural organization and coordination can be important variables in their

electronic behavior [11, 12, 24, 27]. However, those finite-cluster studies are used here as qualitative background rather than as quantitatively equivalent calculations.

Table 1.
Calculated Kohn–Sham electronic gaps of periodic NaCl configurations with different atomic geometries.

Model geometry	Model composition	Number of ions	Calculated Kohn–Sham electronic gap, eV
Linear configuration	NaCl	2	-*
	Na_2Cl_2	4	11.40
	Na_3Cl_3	6	8.449
	Na_6Cl_6	12	10.46
Planar configuration	Na_2Cl_2	4	11.83
	Na_3Cl_3	6	11.46
	Na_4Cl_4	8	11.55
	Na_6Cl_6	12	12.09
Three-dimensional configuration	Na_4Cl_4	8	11.92
	Na_6Cl_6	12	11.12

* The preserved calculation for the two-ion NaCl configuration did not reach self-consistent-field convergence within the specified maximum number of iterations. Therefore, the previously reported electronic-gap value was excluded from the quantitative comparison.

Figure 2 compares the atomic geometries and calculated k-dependent Kohn–Sham electronic spectra of the planar and three-dimensional NaCl configurations. The spectra exhibit clear differences in the distribution and dispersion of the calculated electronic states among the investigated models. As summarized in Table 1, these spectral differences are accompanied by variations in the calculated electronic gaps. The comparison therefore provides a direct illustration of how configurations with different atomic arrangements and periodic simulation cells can exhibit distinct calculated electronic spectra.

The influence of spatial atomic arrangement is particularly evident when configurations with identical chemical composition and ion number are compared. For Na_4Cl_4, the calculated Kohn–Sham electronic gap changes from 11.55 eV in the planar configuration to 11.92 eV in the three-dimensional configuration, corresponding to a difference of 0.37 eV. For Na_6Cl_6, the planar and three-dimensional configurations exhibit calculated gaps of 12.09 and 11.12 eV, respectively, corresponding to a difference of 0.97 eV. Thus, even for models with identical chemical composition and number of ions, differences in spatial atomic arrangement and the corresponding periodic simulation-cell representation are accompanied by appreciable differences in the calculated electronic spectra.

The reciprocal-space labels shown in Figure 2 refer to the Brillouin zones defined by the lattice vectors of the corresponding periodic simulation cells. They are therefore not interpreted as a direct representation of the conventional high-symmetry points and paths of bulk rock-salt NaCl. Comparisons among the spectra are made within the computational representation adopted for each investigated configuration.

In addition to the linear, planar, and three-dimensional NaCl configurations

discussed above, a separate set of structurally and compositionally distinct NaCl models was considered in order to extend the comparison of calculated electronic characteristics. This set includes the compact $Na_{14}Cl_{13}$ configuration, the structurally related $Na_{13}Cl_{12}$ configuration obtained by removal of one Na-Cl pair, the planar Na_5Cl_4 configuration, the elongated $Na_{23}Cl_{22}$ configuration, and the $Na_{22}Cl_{21}$ configuration obtained from the latter by removal of one Na-Cl pair. The corresponding atomic structures are shown in Figure 3.

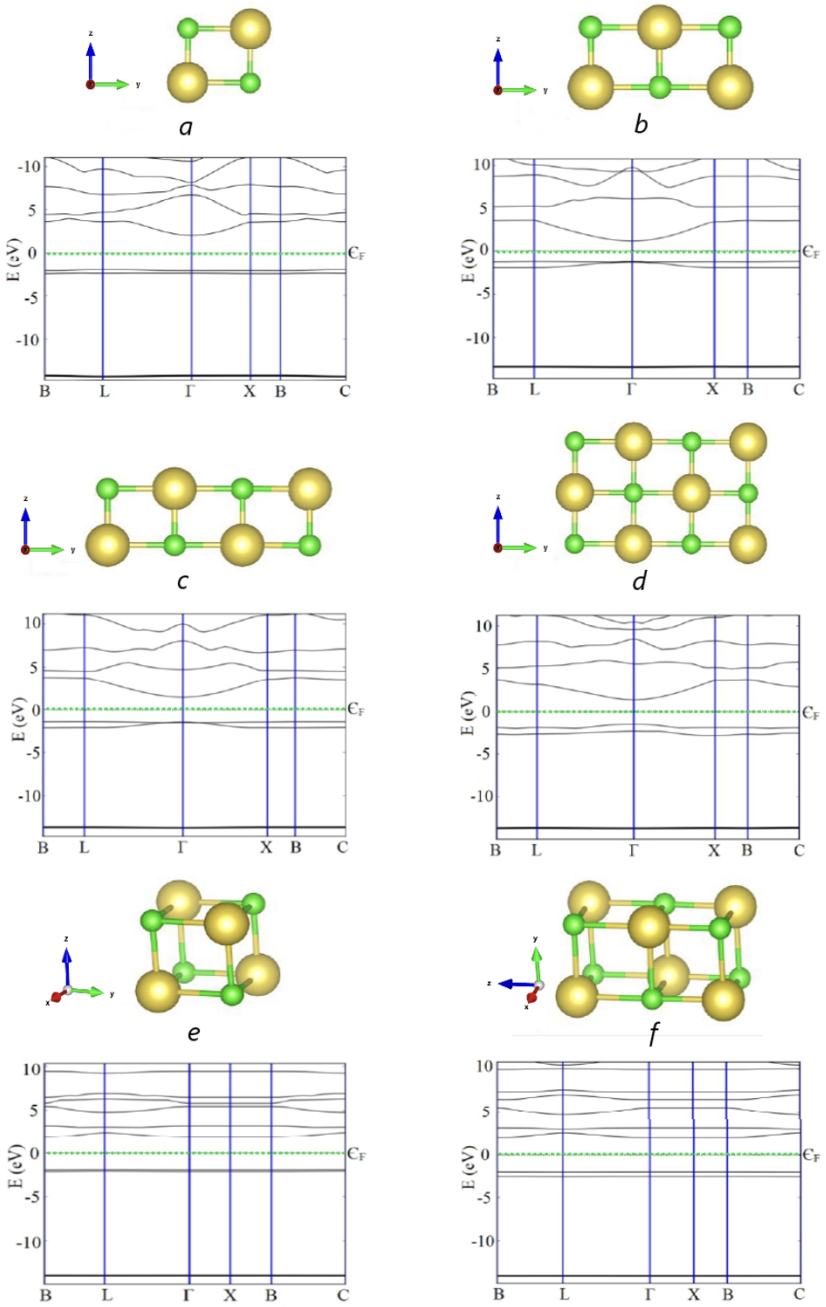

Figure 2. Atomic geometries and calculated k -dependent Kohn–Sham electronic spectra of planar and three-dimensional NaCl configurations represented within periodic simulation cells: (a) Na_2Cl_2 , (b) Na_3Cl_3 , (c) Na_4Cl_4 , and (d) Na_6Cl_6 planar configurations; (e) Na_4Cl_4 and (f) Na_6Cl_6 three-dimensional configurations.

The configurations shown in Figure 3 differ in composition, number of ions, atomic arrangement, and local coordination. Of particular interest are the struc-

turally related $Na_{14}Cl_{13}/Na_{13}Cl_{12}$ and $Na_{23}Cl_{22}/Na_{22}Cl_{21}$ pairs, which represent the corresponding parent and modified configurations before and after removal of one Na-Cl pair. The Na_5Cl_4 model provides an additional geometrically distinct planar configuration. Because removal of an Na-Cl pair changes both the composition and the local atomic environment, differences between the corresponding parent and modified models are interpreted as characteristics of the specific structural and compositional modification rather than as the isolated effect of a single independently varied parameter.

Previous experimental and theoretical investigations of alkali halide clusters have shown that electronic behavior can depend strongly on stoichiometry, the presence of excess electrons, and the atomic arrangement of the cluster [14, 29–30]. In particular, studies of excess-electron alkali halide clusters have examined electron binding, localization, and changes in electronic behavior accompanying variations in composition [14, 31–34]. These findings provide relevant context for examining compositionally modified NaCl models. Nevertheless, the systems considered in those studies differ from the present periodic configurations, and their conclusions regarding localized electronic states cannot be transferred directly to the present results.

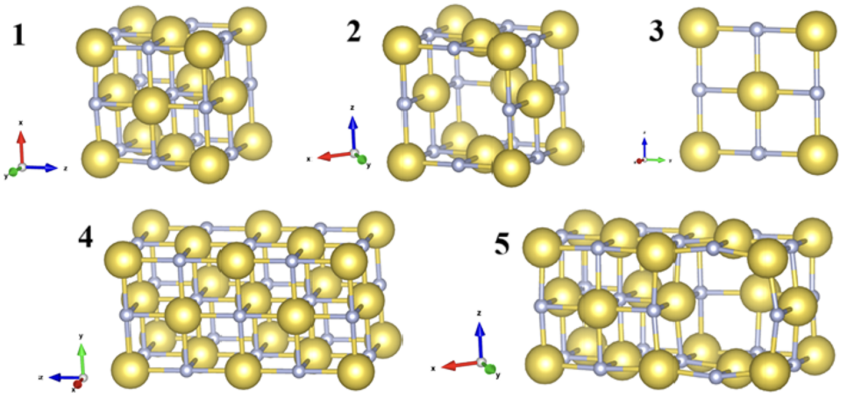

Figure 3. Atomic geometries of the investigated structurally distinct NaCl configurations: (1) $Na_{14}Cl_{13}$, compact $3 \times 3 \times 3$ configuration; (2) $Na_{13}Cl_{12}$, obtained from configuration (1) by removal of one Na–Cl pair; (3) Na_5Cl_4, planar $3 \times 3 \times 3$ configuration; (4) $Na_{23}Cl_{22}$, elongated $3 \times 3 \times 3$ configuration; and (5) $Na_{22}Cl_{21}$, obtained from configuration (4) by removal of one Na-Cl pair. Large yellow spheres represent Na atoms and small purple spheres represent Cl atoms.

The electronic characteristics of the configurations shown in Figure 3 were further examined using the calculated total density of states (DOS). The analysis focuses on differences in the energetic distribution of occupied and unoccupied electronic states among the investigated configurations and, in particular, on changes accompanying the structural and compositional modification of the two related model pairs. The calculated total DOS spectra for Na_5Cl_4, $Na_{13}Cl_{12}$, $Na_{14}Cl_{13}$, $Na_{22}Cl_{21}$, and $Na_{23}Cl_{22}$ are presented in Figure 4.

As shown in Figure 4, the investigated NaCl configurations exhibit both common and model-dependent features in their calculated total DOS spectra. Deep-lying electronic states are present at approximately -18 to -20 eV, while additional occupied states are distributed at higher energies below the corresponding Fermi level. Above ε_F, the distribution and relative spectral weight

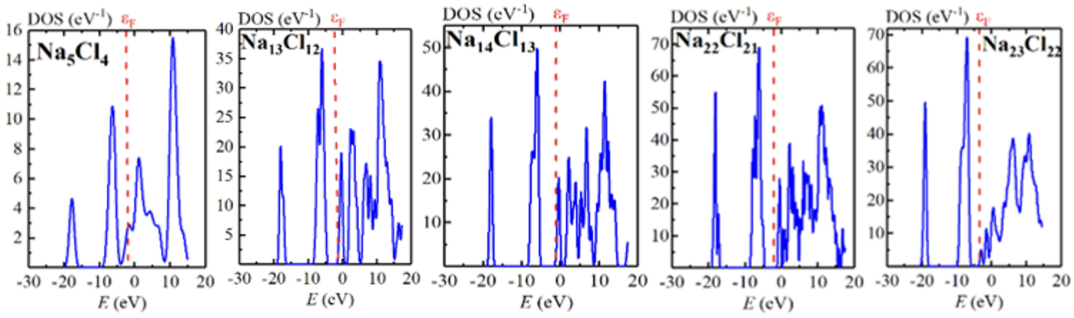

Figure 4. Calculated total DOS spectra of the Na_5Cl_4, $Na_{13}Cl_{12}$, $Na_{14}Cl_{13}$, $Na_{22}Cl_{21}$, and $Na_{23}Cl_{22}$ configurations. The red dashed lines indicate the Fermi energy ε_F.

of the unoccupied states vary among the investigated configurations. Thus, the calculated DOS spectra demonstrate differences in the energetic distribution of electronic states among models with different compositions and atomic arrangements. No orbital-specific assignment of the individual DOS features is made on the basis of the total DOS alone.

A particularly informative comparison is provided by the structurally related $Na_{14}Cl_{13}/Na_{13}Cl_{12}$ and $Na_{23}Cl_{22}/Na_{22}Cl_{21}$ pairs. Removal of one Na-Cl pair does not eliminate the principal features of the total DOS spectrum but is accompanied by changes in the distribution and relative spectral weight of electronic states on both sides of the electronic gap. The magnitude and spectral character of these changes differ between the two structural pairs, demonstrating that removal of an Na-Cl pair is accompanied by model-dependent changes in the calculated electronic-state distribution.

It should be emphasized that the total DOS provides information about the energetic distribution of the calculated electronic states but does not, by itself, determine their atomic-orbital character, spatial localization, or associated charge distribution. Therefore, the spectral modifications observed after removal of an Na-Cl pair are interpreted here as changes in the electronic-state distribution of the corresponding modified periodic configuration. In the absence of atom- or orbital-resolved DOS, charge-density analysis, or other spatially resolved electronic-structure calculations, these changes are not assigned to a specific localized defect state, vacancy-related electronic center, or particular charge state.

To further examine the electronic characteristics of the structurally modified NaCl model, the $Na_{13}Cl_{12}$ configuration obtained from the parent $Na_{14}Cl_{13}$ configuration by removal of one Na-Cl pair was analyzed separately. In addition to its total DOS, the k-dependent Kohn–Sham electronic spectrum was calculated for this configuration and is presented in Figure 5. The calculated spectrum yields a minimum Kohn–Sham electronic gap of approximately 9.01 eV between the highest occupied and lowest unoccupied calculated states.

The calculated Kohn–Sham electronic gap of the $Na_{13}Cl_{12}$ configuration is approximately 9.01 eV and characterizes the specific structurally and compositionally modified periodic configuration considered here. Together with the DOS changes shown in Figure 4, the calculated spectrum shows that removal of an Na-Cl pair from the parent configuration is accompanied by a modification of

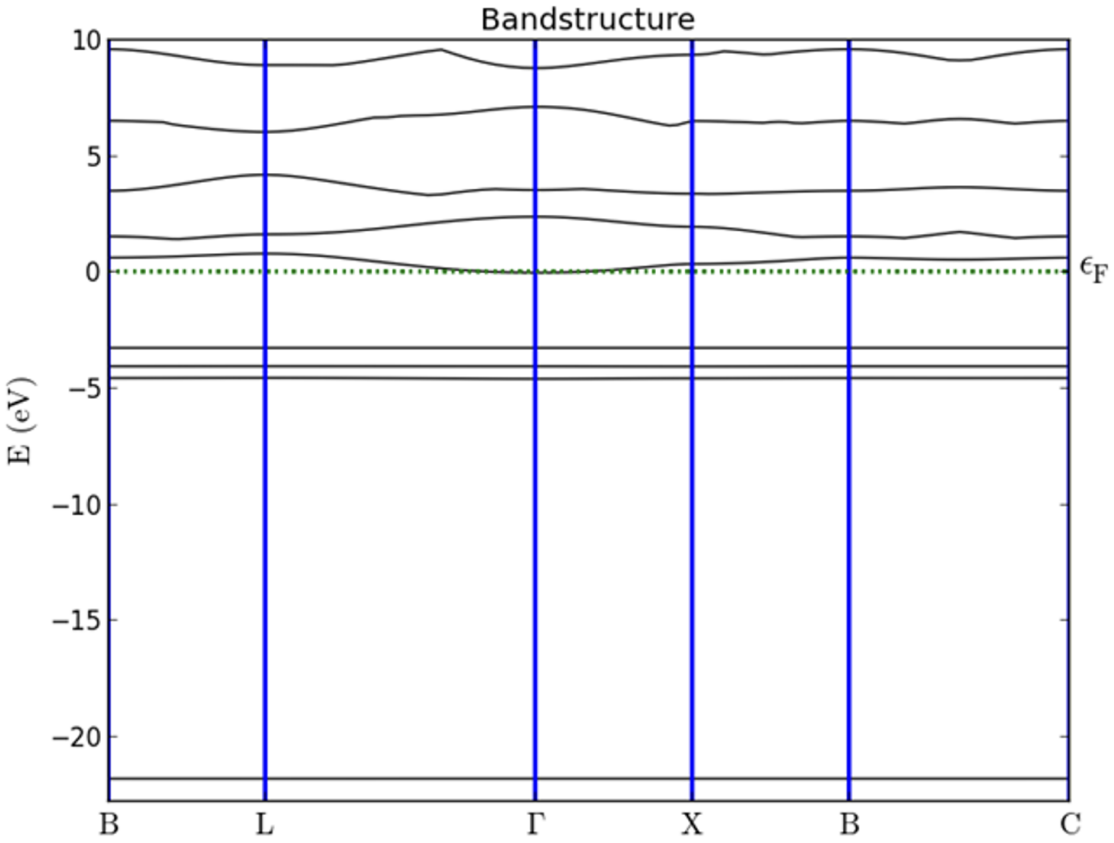

Figure 5. Calculated k-dependent Kohn–Sham electronic spectrum of the $Na_{13}Cl_{12}$ configuration obtained by removal of one Na-Cl pair from the parent $Na_{14}Cl_{13}$ configuration.

the electronic-state distribution. However, in the absence of charge-density, atom- or orbital-resolved, or other spatially resolved electronic-structure analyses, these changes cannot be assigned to a specific localized defect state or vacancy-related electronic center.

Although the calculated value of 9.01 eV for the $Na_{13}Cl_{12}$ configuration is numerically close to the commonly reported experimental bulk-gap scale of approximately 8.6 eV [5–8], the two quantities are not directly equivalent. The calculated value refers to the Kohn–Sham electronic gap of a specific non-stoichiometric periodic configuration, whereas the experimental value refers to bulk crystalline NaCl. Their numerical proximity is therefore not used as a validation criterion for the present computational model.

Periodic NaCl nanotubes were investigated as a separate structural class. The nanotube series considered in the present work consists of the $(4,1)$, $(5,1)$, and $(6,1)$ configurations, with the second index n fixed at 1 and the first index m increasing from 4 to 6. As described in the Materials and Methods section, these models also differ in the number of atoms and simulation-cell dimensions. Figure 6 shows the atomic structure and periodic simulation cell of the representative $(5,1)$ NaCl nanotube configuration.

The nanotube configurations were represented within periodic simulation cells whose dimensions were defined separately for each model, as described in the Materials and Methods section. Prior to the electronic-structure calculations,

the nanotube geometries were optimized using the classical interatomic-potential procedure described above. The optimized configurations were subsequently used for DFT calculations of the k-dependent Kohn–Sham electronic spectra and total density of states. As noted above, the geometry optimization is used here only to obtain the structural configurations employed in the electronic-structure calculations and is not interpreted as evidence of dynamical or thermodynamic stability.

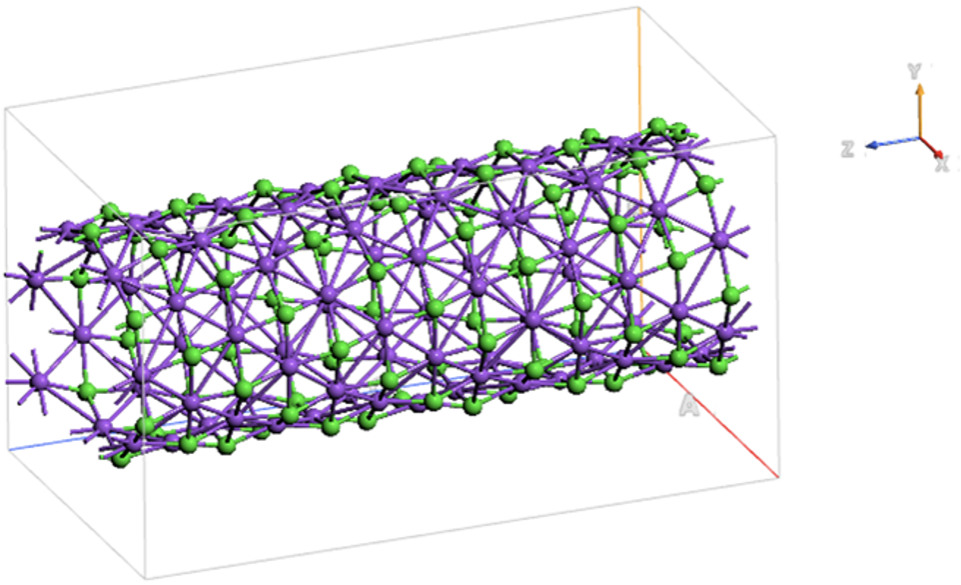

Figure 6. Atomic structure and periodic simulation cell of the representative $(5,1)$ NaCl nanotube configuration used in the electronic-structure calculations.

The electronic characteristics of the investigated nanotube models were analyzed using their calculated k-dependent Kohn–Sham electronic spectra. Figure 7 presents the calculated spectrum of the $(4,1)$ NaCl nanotube configuration, together with an enlarged view of the energy region near the Fermi level. The reciprocal-space path used for the calculation is specified in the Materials and Methods section.

The calculated electronic spectra of the investigated NaCl nanotube configurations exhibit a clear separation between the occupied and unoccupied Kohn–Sham states. The calculated electronic gaps are approximately 6.40, 5.32, and 5.00 eV for the $(4,1)$, $(5,1)$, and $(6,1)$ configurations, respectively. Thus, within the investigated nanotube series, the calculated electronic gap decreases systematically as the first geometrical index increases from $m = 4$ to $m = 6$, while $n = 1$ remains fixed.

The decrease in the calculated electronic gap from 6.40 eV for the $(4,1)$ configuration to 5.00 eV for the $(6,1)$ configuration corresponds to an overall change of 1.40 eV, or approximately 22% relative to the $(4,1)$ value. Although n remains fixed at 1 throughout the investigated series, this trend should not be attributed exclusively to the increase in m. The three nanotube models also differ substantially in the number of atoms and simulation-cell dimensions, as described in the Materials and Methods section. The observed decrease in the electronic gap is therefore interpreted as a systematic trend within the specific sequence of

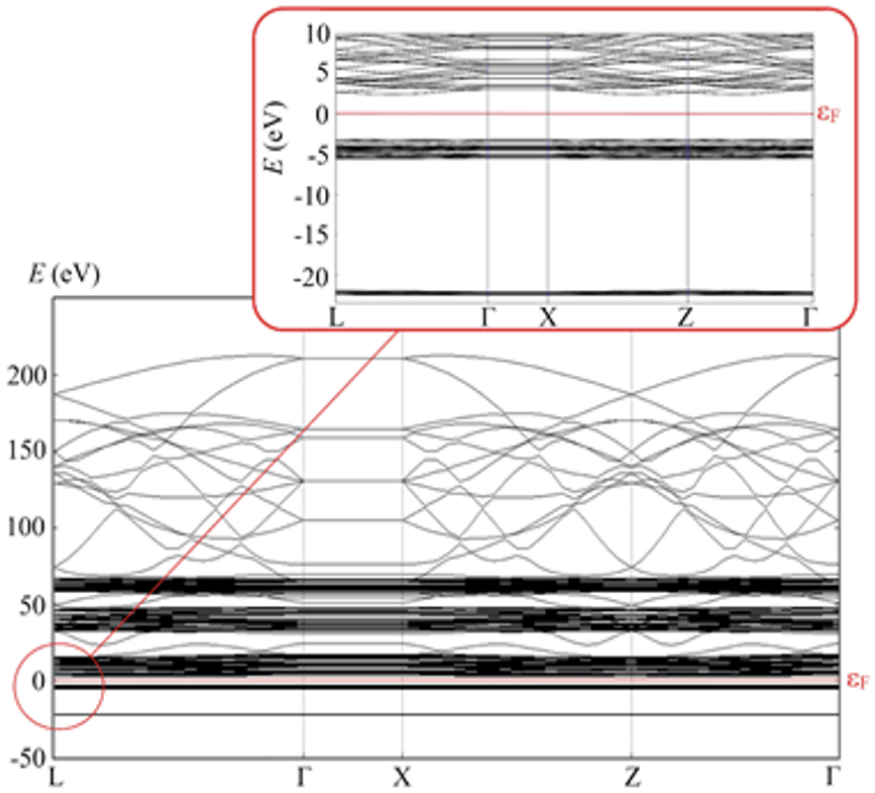

Figure 7. Calculated k-dependent Kohn–Sham electronic spectrum of the $(4,1)$ NaCl nanotube configuration. The inset shows an enlarged view of the electronic states in the vicinity of the Fermi level ε_F.

$(4,1)$, $(5,1)$, and $(6,1)$ NaCl nanotube models rather than as an independently established dependence of the electronic gap on a single geometrical parameter.

Previous computational studies of alkali halide nanotubes provide a relevant framework for interpreting these observations. Investigations of tubular ionic structures have demonstrated that geometrical organization and composition can affect calculated electronic properties [16, 17]. However, direct numerical comparison of electronic gaps requires consideration of differences in composition, structural models, and computational settings. Accordingly, the present NaCl nanotube gaps are discussed as results of the specific periodic DFT-LCAO models employed here rather than as universally transferable characteristics of NaCl nanotubes.

To further compare the electronic characteristics of the investigated nanotube models, the total DOS spectra were analyzed for the $(4,1)$, $(5,1)$, and $(6,1)$ NaCl configurations. Within this series, n remains fixed at 1, whereas the first geometrical index m increases from 4 to 6. However, the models also differ in the number of atoms and simulation-cell dimensions; therefore, the resulting DOS variations are considered as trends within the investigated nanotube series rather than as an isolated dependence on m. The calculated DOS spectra are presented in Figure 8 over the energy range from approximately -30 to 20 eV.

As shown in Figure 8, all three nanotube configurations exhibit a region of strongly reduced density of states between the dominant occupied and unoccupied electronic states in the vicinity of the Fermi level, consistent with the finite

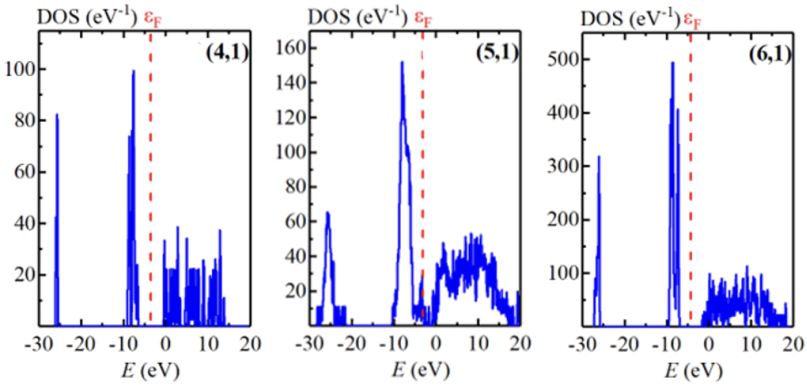

Figure 8. Calculated total DOS spectra of the $(4,1)$, $(5,1)$, and $(6,1)$ NaCl nanotube configurations. The red dashed lines indicate the Fermi energy ε_F.

electronic gaps obtained from the k-dependent spectra. At the same time, the DOS profiles show model-dependent differences in the energetic distribution and shape of the occupied and unoccupied states. These spectral differences accompany the variation in the calculated electronic gaps across the $(4,1)$, $(5,1)$, and $(6,1)$ nanotube series.

The comparison of the three nanotube models shows that changes in the calculated electronic gap are accompanied by changes in the overall DOS profile. However, differences in the absolute DOS intensity should not be interpreted directly as changes in electronic localization, bond strength, or the intrinsic density of states per atom. The $(4,1)$, $(5,1)$, and $(6,1)$ computational models contain different numbers of atoms and therefore different total numbers of electronic states. Consequently, the present comparison is focused primarily on the energetic distribution of the DOS features and the calculated electronic gaps rather than on the absolute magnitude of the total DOS.

Taken together, the k-dependent electronic spectra and total DOS results reveal systematic differences among the investigated NaCl nanotube configurations. All three models exhibit finite calculated electronic gaps, while the positions and distributions of the DOS features vary across the $(4,1)$, $(5,1)$, and $(6,1)$ series. These results demonstrate that the calculated electronic characteristics differ systematically among the investigated nanotube models; however, because the models vary simultaneously in geometrical index, number of atoms, and simulation-cell dimensions, the observed differences are not attributed exclusively to a single structural parameter.

4. Conclusion

In this work, the electronic characteristics of NaCl structures with different atomic geometries were investigated within periodic computational representations. The considered models included linear, planar, three-dimensional, structurally and compositionally modified NaCl configurations, as well as periodic NaCl nanotubes. Analysis of the calculated k-dependent Kohn–Sham electronic spectra

and total density of states demonstrates systematic variations in the electronic characteristics among models with different atomic arrangements and structural representations.

For the linear, planar, and three-dimensional NaCl configurations included in the quantitative comparison, the calculated Kohn–Sham electronic gaps range from approximately 8.45 to 12.09 eV and show no simple monotonic dependence on the number of ions in the simulation cell. Configurations with identical composition but different spatial atomic arrangements also exhibit different calculated gaps. In particular, the planar and three-dimensional Na_4Cl_4 configurations exhibit gaps of 11.55 and 11.92 eV, respectively, whereas the corresponding values for Na_6Cl_6 are 12.09 and 11.12 eV. These comparisons show that composition and ion number alone are insufficient to characterize the calculated electronic spectra of the investigated periodic NaCl models and that differences in atomic arrangement and the corresponding periodic simulation-cell representation must also be taken into account.

For the structurally and compositionally modified NaCl configurations, comparison of the total DOS spectra shows that removal of an Na-Cl pair from the structurally related $Na_{14}Cl_{13}/Na_{13}Cl_{12}$ and $Na_{23}Cl_{22}/Na_{22}Cl_{21}$ model pairs is accompanied by changes in the energetic distribution and relative spectral weight of the calculated electronic states. For the $Na_{13}Cl_{12}$ configuration, the calculated k-dependent spectrum yields a Kohn–Sham electronic gap of approximately 9.01 eV. This value is interpreted as a characteristic of the specific non-stoichiometric periodic configuration and not as a direct theoretical estimate of the experimental fundamental gap of bulk crystalline NaCl. Because no atom- or orbital-resolved DOS, charge-density, or other spatially resolved electronic-structure analyses were performed, the observed spectral changes are not assigned to a specific localized defect state, vacancy-related electronic center, or particular charge state.

For the periodic NaCl nanotube models, the calculated Kohn–Sham electronic gaps decrease systematically from approximately 6.40 eV for the $(4,1)$ configuration to 5.32 eV for $(5,1)$ and 5.00 eV for $(6,1)$, corresponding to an overall decrease of 1.40 eV between the $(4,1)$ and $(6,1)$ models. The total DOS spectra likewise exhibit model-dependent differences in the energetic distribution of electronic states. Although n remains fixed at 1 while m increases from 4 to 6, the three models also differ in the number of atoms and simulation-cell dimensions. The observed changes in the electronic gaps and DOS are therefore interpreted as systematic trends within the investigated nanotube series rather than as an independently established dependence on m alone. Differences in the absolute magnitude of the total DOS are not interpreted as direct evidence of changes in electronic localization, bond strength, or the intrinsic density of states per atom.

Overall, the present calculations establish systematic relationships between structural representation and the calculated electronic characteristics of the investigated NaCl models. Within the adopted periodic computational framework, neither ion number nor composition alone provides a sufficient descriptor of the calculated electronic spectrum; differences in atomic arrangement and simulation-cell representation are also associated with substantial variations in the Kohn–

Sham electronic gaps and DOS profiles. The conclusions of the present work are restricted to the electronic-structure descriptors directly obtained from the calculations. No conclusions regarding dynamical or thermodynamic stability are drawn, because phonon or vibrational-frequency calculations, finite-temperature molecular-dynamics simulations, and formation- or cohesive-energy analyses were not performed. Further atom- and orbital-resolved electronic-structure calculations, charge-density analyses, and appropriate stability calculations would be required to determine the microscopic origin of particular electronic states and to assess the dynamical and thermodynamic stability of the investigated configurations.

Acknowledgments

This research was funded by the Ministry of Science and Higher Education of the Republic of Kazakhstan by project No. 09057911 "Experimental studies of the mechanisms of luminescence of KI, RbI and CsI crystals at the activation by cations-homologues and low temperature deformation".

References

[1] N.W. Ashcroft, N.D. Mermin, Solid State Physics (Holt, Rinehart and Winston: New York, 1976) 826 p.
[2] H.J.F. Jansen et al., Phys. Rev. B **33** (1986) 8629–8631. [*CrossRef*]
[3] L.J. Page et al., Phys. Rev. B **1** (1970) 3472–3479. [*CrossRef*]
[4] C.Y. Fong et al., Phys. Rev. Lett. **21** (1968) 22–25. [*CrossRef*]
[5] D.M. Roessler et al., Phys. Rev. **166** (1968) 599–606. [*CrossRef*]
[6] F. Bechstedt et al., Phys. Rev. B **72** (2005) 245114. [*CrossRef*]
[7] R. Haensel et al., Phys. Rev. Lett. **23** (1969) 530–532. [*CrossRef*]
[8] H. Zhang et al., Phys. Rev. B **50** (1994) 70–74. [*CrossRef*]
[9] F.J. Himpsel et al., Phys. Rev. B **17** (1978) 2537–2544. [*CrossRef*]
[10] T.P. Martin, Phys. Rep. **95** (1983) 167–199. [*CrossRef*]
[11] A. Aguado et al., Phys. Rev. B **56** (1997) 15353–15360. [*CrossRef*]
[12] H. Kabrede et al., J. Phys. Chem. B **106** (2002) 10089–10095. [*CrossRef*]
[13] R.L. Whetten, Acc. Chem. Res. **26** (1993) 49–56. [*CrossRef*]
[14] E.C. Honea et al., Phys. Rev. Lett. **63** (1989) 394–397. [*CrossRef*]
[15] F.A. Fernandez-Lima et al., Nucl. Instrum. Methods Phys. Res. B **273** (2012) 102–104. [*CrossRef*]
[16] L.N. Myasnikova et al., Latv. J. Phys. Tech. Sci. **56** (2019) 49–56. [*CrossRef*]
[17] F.A. Fernandez-Lima et al., J. Phys. Chem. C **116** (2012) 4965–4969. [*CrossRef*]
[18] A.S. Istlyaup et al., Low Temp. Phys. **50** (2024) 569–573. [*CrossRef*]
[19] Y.J. Twu et al., Phys. Rev. B **42** (1990) 5306–5316. [*CrossRef*]
[20] K. Ohshimo et al., J. Phys. Chem. A **118** (43) (2014) 9970–9975. [*CrossRef*]
[21] A.S. Istlyaup et al., Low Temp. Phys. **50** (2024) 898–904. [*CrossRef*]
[22] F. Bloch, Z. Phys. **52** (1929) 555–600. [*CrossRef*]
[23] Atomistix ToolKit Manual, Version 2015.1 (QuantumWise A/S, 2015).

[24] H.J. Monkhorst et al., Phys. Rev. B **13** (1976) 5188–5192. [*CrossRef*]
[25] A.A. Aldongarov et al., Eurasian J. Phys. Funct. Mater. **4** (2020) 255–260. [*CrossRef*]
[26] P. Hohenberg et al., Phys. Rev. **136** (1964) B864–B871. [*CrossRef*]
[27] W. Kohn et al., Phys. Rev. **140** (1965) A1133–A1138. [*CrossRef*]
[28] J.P. Perdew et al., Phys. Rev. Lett. **77** (1996) 3865–3868. [*CrossRef*]
[29] M. Lintuluoto, J. Mol. Struct. THEOCHEM **540** (2001) 177–192. [*CrossRef*]
[30] R.D. Beck et al., Science **253** (1991) 879–883. [*CrossRef*]
[31] A.D. Davletshina et al., Eurasian J. Phys. Funct. Mater. **8** (4) (2024) 194–198. [*CrossRef*]
[32] G. Rajagopal et al., Phys. Rev. Lett. **64** (1990) 2933–2936. [*CrossRef*]
[33] G. Rajagopal et al., Phys. Rev. Lett. **67** (1991) 727–730. [*CrossRef*]
[34] U. Landman et al., Phys. Rev. Lett. **54** (1985) 1860–1863. [*CrossRef*]